The Unified-FFT Algorithm for Fast Electromagnetic Analysis of Planar Integrated Circuits Printed on Layered Media Inside a Rectangular Enclosure

Brian J. Rautio, *Member, IEEE*, Vladimir I. Okhmatovski, *Senior Member, IEEE*, Andreas C. Cangellaris, *Fellow, IEEE*, James C. Rautio, *Fellow, IEEE*, and Jay Kyoon Lee, *Senior Member, IEEE*

***Abstract*—The unified fast Fourier transform (UFFT) methodology is proposed for fast method of moments analysis of dense integrated circuits embedded in layered media inside perfectly electric conducting or perfectly magnetic conducting enclosures of rectangular cross section. The pre-corrected fast Fourier transform (FFT) method is modified to handle the dyadic Green's function (DGF) of shielded layered media through factorization of the DGF into four convolution/correlation terms enabling fast matrix solve operations (MSOs). Calculation of the impedance matrix elements in the form of an infinite series of waveguide modes is cast into the form of a 2-D discrete Fourier transform allowing for fast FFT-accelerated matrix fill operations (MFOs). Fast FFT-enhanced MSOs and MFOs used in conjunction form the UFFT method. The computational complexity and memory requirements for the proposed UFFT solver scale as $O(N \log N)$ and $O(N)$, respectively, where N is the number of unknowns in the discrete approximation of the governing integral equation. New criteria specific to shielded circuits for the projection of the current expansion functions on a uniform FFT grid are developed. The accuracy and efficiency of the solver is demonstrated through its application to multiple examples of full-wave analysis of large planar circuits.**

***Index Terms*—Computer-aided design (CAD), CAD algorithms and techniques, fast algorithms, numerical analysis, RF integrated circuit (RFIC) modeling.**

I. Introduction

DENSE PLANAR and quasi-planar integrated circuits (ICs) are becoming common in the development of multi-layered packages and substrates for the realization of compact system-in-package (SIP) and system-on-chip (SOC) multi-function designs. The interconnect density in multi-layered substrates for such systems is high such that the number of unknowns, N, in the matrix approximation of the electromagnetic equations for these problems is on the order of hundreds of thousands or more. While simple and reliable, full matrix inverse solution of these dense matrices is computationally prohibitive. Further, while application of iterative conjugate gradient (CG) [1] methods reduces processing requirements, the dense nature of the method of moments (MoM) matrix results in memory and operations that unfortunately both scale as $O(N^2)$.

To address complexity and establish a computationally efficient approach to electromagnetic characterization of high-density and/or electrically large planar circuits, there have been several classes of fast algorithms developed over the last two decades. Among these methods are kernel dependent iterative fast methods, such as the multi-level fast multipole algorithm (MLFMA) [2], [3], pre-corrected fast Fourier transform (PFFT) algorithm (also known as the adaptive integral method (AIM) [4]–[10]), which notably allows for off-grid discretization, conjugate gradient fast Fourier transform (CG-FFT) algorithm [11]–[14] which must conform to a grid, integral equation fast Fourier transform (IE-FFT) method [15], sparse-matrix/canonical grid (SM/CG) method [16], and kernel-independent algorithms, such as iterative QR- and SVD-based compression techniques [17]–[19], iterative [20], [21] and direct [22] H-matrix based methods, iterative adaptive-cross-approximation method [23], [24], and iterative wavelet-based compression method [25]. Though the latter group of kernel-independent algorithms can be applied to acceleration of MoM solutions in conjunction with complex dyadic Green's functions (DGFs) of layered media and/or perfect enclosures, special implementations are required to produce sufficient accuracy of results [26]. Conversely, full-wave algorithms, such as the MLFMA, PFFT, and CG-FFT, which natively retain both accuracy and efficiency in capturing full-wave physics, require significant and rarely implemented modification for complex media. The MLFMA has been extended to handle full-wave layered kernels in its modification, fast inhomogeneous plane-wave algorithm [27], [28]; however, it does not rigorously demonstrate rigorous error control beyond two to three significant figures. The MLFMA has also been extended for the case of static layered kernels [29], [30], and rectangular enclosures in the absence of layered media [31].

In the class of fast Fourier transform (FFT)-based algorithms, several modifications of the algorithm have been developed for

Manuscript received November 23, 2013; revised March 02, 2014; accepted March 31, 2014. Date of publication April 14, 2014; date of current version May 02, 2014.

B. J. Rautio and J. K. Lee are with the Department of Electrical Engineering and Computer Science, Syracuse University, Syracuse, NY 13244 USA (e-mail: bjrautio@syr.edu).

V. I. Okhmatovski is with the Department of Electrical and Computer Engineering, University of Manitoba, Winnipeg, MB, Canada R3T 5V6.

A. C. Cangellaris is with the Department of Electrical and Computer Engineering, University of Illinois at Urbana-Champaign, Urbana, IL 61801 USA.

J. C. Rautio is with Sonnet Software, North Syracuse, NY 13212 USA.

Color versions of one or more of the figures in this paper are available online at http://ieeexplore.ieee.org.

Digital Object Identifier 10.1109/TMTT.2014.2315594

unshielded layered media [32]–[36]. The attempt of generalizing the PFFT method to the case of shielded stratified media has been made [37]. This method, however, fell short of expectations due to the large computational complexity associated with matrix fill operations (MFOs) with only moderate size problems having been analyzed. Issues in [37] are remedied in this work through application of a previously unpublished FFT-enhanced algorithm for MFO developed by Rautio and implemented for rapid MFO in Sonnet ***em*** [38]. This MFO algorithm is shown to scale as $O(N \log N)$. Additionally, the previously developed PFFT generalization for shielded stratified media [37] has been further advanced through introduction of a more accurate method for basis function projection onto the FFT grid utilizing waveguide mode matching instead of standard multipole reproduction criteria [5]. The PFFT algorithm for fast handling of the matrix solve operations (MSOs) has also been generalized to the handling of both perfectly electric conducting (PEC) and mixed PEC/perfectly magnetic conducting (PMC) types of enclosures. As MFO and MSO are the two main time-consuming operations in the MoM solution of the electric field integral equation (EFIE), the novel use of FFT-accelerated versions of both in conjunction creates the unified fast Fourier transform (UFFT) methodology for the expedient MoM solution of planar electromagnetic analysis in the shielded layered environment. This work identifies, develops, tests, and shows the meaningful relationship between the two existing FFT-enhanced operations. Moreover, the FFT enhanced MFO in [38] is detailed for the first time.

For clarity, it should be explained that this is expressly a 3-D planar solver as opposed to an arbitrary 3-D solver. It accepts limitation of simulation capability to predominantly planar structures, such as those printed on printed circuit boards (PCBs) and ICs, in exchange for more efficient meshing of the structure. Note that while this generally reduces the number of unknowns significantly, it does not reduce the complexity of the algorithm per unknown.

II. EFIE and Its MOM Discretization

Well-known MoM techniques discretizing the EFIE [1] lead to the following matrix equation:

$$\begin{bmatrix} \mathbf{Z}^{xx} & \mathbf{Z}^{xy} \\ \mathbf{Z}^{yx} & \mathbf{Z}^{yy} \end{bmatrix} \begin{bmatrix} \mathbf{I}^{x} \\ \mathbf{I}^{y} \end{bmatrix} = \begin{bmatrix} \mathbf{V}^{x} \\ \mathbf{V}^{y} \end{bmatrix} \tag{1}$$

where the vector $\mathbf{I}$ is the solution and the matrix and right-hand-side elements are given by

$$\begin{aligned} Z_{ij}^{\alpha\beta} &= \int_{S_i} t_i^{\alpha}(\vec{r}) \int_{S_j} G^{\alpha\beta}(\vec{r};\vec{r}\,')\, b_j^{\beta}(\vec{r}\,')\, ds' \\ V_i^{\alpha} &= \int_{S_i} t_i^{\alpha}(\vec{r}) E^{\alpha,inc}(\vec{r})\, ds, \\ &\alpha,\beta = x,y; \quad i,j = 1,\ldots,N^{\alpha,\beta}. \end{aligned} \tag{2}$$

The shorthand notation $\mathbf{Z} \cdot \mathbf{I}$ is used to denote the matrix-vector product of (1). For large or dense circuits with unknowns on the order of tens of thousands or more, iterative methods (e.g., CG) are needed to avoid $O(N^3)$ complexity in solving (1) via LU decomposition [39]. The computational complexity of such methods is dominated by the $O(N^2)$ operations of the matrix-vector product $\mathbf{Z}\cdot\mathbf{I}$ at each iteration. The memory storage also scales as $O(N^2)$ as the dense matrix $\mathbf{Z}$ must be calculated explicitly and stored. The objective of the UFFT method is to further reduce CPU scaling from $O(N^2)$ to $O(N \log N)$ and memory from $O(N^2)$ to $O(N)$. Similar to other fast algorithms, the UFFT addresses this complexity by splitting $\mathbf{Z}\cdot\mathbf{I}$ into "near-zone" interactions and "far-zone" interactions. This split may be written in the form

$$\mathbf{Z}\cdot\mathbf{I} = \mathbf{Z}_{\mathrm{MoM}}^{\mathrm{near}}\cdot\mathbf{I} + \hat{\mathbf{Z}}^{\mathrm{far}}\cdot\mathbf{I} = \mathbf{Z}_{\mathrm{MoM}}^{\mathrm{near}}\cdot\mathbf{I} + (\hat{\mathbf{Z}}\cdot\mathbf{I} - \hat{\mathbf{Z}}^{\mathrm{near}}\cdot\mathbf{I}) \tag{3}$$

where $\hat{\mathbf{Z}}$ denotes impedance matrix elements from the projected geometry without pre-correction, and $\mathbf{Z}$ denotes pre-correction and pre-corrected matrix elements. $\mathbf{Z}_{\mathrm{MoM}}^{\mathrm{near}}\cdot\mathbf{I}$ contains the interactions between closely spaced elements, separated by distances less than some threshold distance. These interactions are calculated using the standard integrals (2) resulting from the MoM process. Even though the matrix $\mathbf{Z}_{\mathrm{MoM}}^{\mathrm{near}}$ is sparse and the computational complexity of $\mathbf{Z}_{\mathrm{MoM}}^{\mathrm{near}}\cdot\mathbf{I}$ is $O(N)$, the specificity of a MoM implementation for planar circuits in shielded layered media is such that the constant in front of $O(N)$ is very large when the matrix elements are calculated through direct summation of waveguide mode contributions. In Section III, we describe an FFT-based algorithm, which drastically reduces the matrix $\mathbf{Z}_{\mathrm{MoM}}^{\mathrm{near}}$ fill operations to $O(N \log N)$ with a small multiplying factor.

In Section IV, we describe how the "far-zone" interactions modeled by the matrix-vector product $\hat{\mathbf{Z}}^{\mathrm{far}}\cdot\mathbf{I}$ can be evaluated in $O(N \log N)$ operations via the PFFT algorithm when modified with a DGF for layered media in a shielding waveguide, thus forming the fast MSOs of the UFFT.

III. FFT-Enhanced MFOs of UFFT

The steps of the algorithm are described for the evaluation of example matrix element Z_{pq}^{xx} in a Galerkin MoM for rooftop basis and testing functions $b_q^x(\vec{r})$ and $t_p^x(\vec{r})$ [40] that conform to a regular grid. The grid-spanning waveguide cross section with M divisions from 0 to a and N divisions from 0 to b is introduced. Analytic evaluation of the integrals of basis and testing functions in (2), followed by reordering of summation as in [41], produces the following form:

$$\begin{aligned} Z_{pq}^{xx} = \sum_{m=1}^{M/2-1} \sum_{n=1}^{N/2-1} & \sin\frac{n\pi n_p}{N} \sin\frac{n\pi n_q}{N} \cos\frac{m\pi m_p}{M} \\ & \times \cos\frac{m\pi m_q}{M} h_{mn}^{xx} \end{aligned} \tag{4}$$

where $(m_p a/M, n_p b/N)$ and $(m_q a/M, n_q b/N)$ are the centers of the test and basis functions, respectively. Coefficients h_{mn}^{xx} in (4) are defined as an infinite double series that can be calculated to desired precision [41]. These coefficients are independent of the locations of test and basis functions and are solely defined by dimensions of the waveguide and the layered substrate. Using identities $\sin x = [\exp(jx) - \exp(-jx)]/2j$ and

$\cos x = [\exp(jx) + \exp(-jx)]/2$ for each of the sine and cosine functions in (4) obtains the matrix element in the form

$$\begin{aligned} Z_{pq}^{xx} = & \sum_{m=-M/2-1}^{M/2+1} \sum_{n=-N/2}^{\frac{N}{2}} \exp\left[j\frac{n\pi(n_p-n_q)}{N}\right] \\ & \times \exp\left[j\frac{m\pi(m_p-m_q)}{M}\right] h_{mn}^{xx} \\ & + \sum_{m=-M/2-1}^{M/2+1} \sum_{n=-N/2}^{\frac{N}{2}} \exp\left[j\frac{n\pi(n_p-n_q)}{N}\right] \\ & \times \exp\left[j\frac{m\pi(m_p+m_q)}{M}\right] h_{mn}^{xx} \\ & + \sum_{m=-M/2-1}^{M/2+1} \sum_{n=-N/2}^{\frac{N}{2}} \exp\left[j\frac{n\pi(n_p+n_q)}{N}\right] \\ & \times \exp\left[j\frac{m\pi(m_p-m_q)}{M}\right] h_{mn}^{xx} \\ & + \sum_{m=-M/2-1}^{M/2+1} \sum_{n=-N/2}^{\frac{N}{2}} \exp\left[j\frac{n\pi(n_p+n_q)}{N}\right] \\ & \times \exp\left[j\frac{m\pi(m_p+m_q)}{M}\right] h_{mn}^{xx}. \end{aligned} \tag{5}$$

The matrix element Z_{pq}^{xx} in (5) is seen to be the sum of the four terms, each of which is in the form of a 2-D discrete Fourier transform (DFT). Further, each of the DFTs have convolution/correlation dependence on the indices defining spatial positions of the basis and testing functions. Thus, any matrix element can be obtained by first calculating matrix $\mathbf{H}^{xx}$ using FFT as

$$\begin{aligned} H_{\mu\nu}^{xx} &= \sum_{m=-M/2}^{M/2-1} \sum_{n=-N/2}^{N/2-1} \exp\left[j\frac{n\pi\nu}{N}\right] \exp\left[j\frac{m\pi\mu}{M}\right] h_{mn}^{xx} \\ &= \mathrm{FFT}\left\{h_{mn}^{xx}\right\} \end{aligned} \tag{6}$$

for $\mu = -M/2, \ldots, M/2-1$, $\nu = -N/2, \ldots, N/2-1$, and then calculating the matrix element values as

$$\begin{aligned} Z_{pq}^{xx} = H_{m_p-m_q,n_p-n_q}^{xx} + H_{m_p-m_q,n_p+n_q}^{xx} + H_{m_p+m_q,n_p-n_q}^{xx} \\ + H_{m_p+m_q,n_p+n_q}^{xx}. \end{aligned} \tag{7}$$

Note that for indices $m_p \pm m_q$ and $n_p \pm n_q$ outside the range $-M/2, \ldots, M/2-1$ and $-N/2, \ldots, N/2-1$, values are calculated according to periodicity of the DGF, which is reflected in matrix $\mathbf{H}^{xx}$. This calculation scales as $O[M_b N_b \log(M_b N_b)]$ operations due to FFT, where M_b and N_b are the number of discretization cells on the x- and y-axis, respectively. Subsequently, all Z_{pq}^{xx} matrix elements can be calculated from $\mathbf{H}^{xx}$ via (7). In case of the UFFT and other matrix-free methods, only $O(N)$ matrix elements $\mathbf{Z}_{\mathrm{MoM}}^{\mathrm{near}}$ corresponding to the near interactions need to be computed, as opposed to $O(N^2)$ in methods, where the matrix is explicitly stored. Thus, calculation of $\mathbf{Z}_{\mathrm{MoM}}^{\mathrm{near}}$ requires $O[M_b N_b \log(M_b N_b)]$ operations with the proposed FFT enhanced approach. In a similar manner, matrices $\mathbf{H}^{xy}$, $\mathbf{H}^{yx}$, and $\mathbf{H}^{yy}$ are computed for evaluation of the remaining three blocks $\mathbf{Z}^{xy}$, $\mathbf{Z}^{yx}$, and $\mathbf{Z}^{yy}$ of the impedance matrix $\mathbf{Z}$ in the general form

$$\begin{aligned} Z_{pq}^{\alpha\beta} = s_1^\beta H_{m_p-m_q,n_p-n_q}^{\alpha\beta} + s_2^\beta H_{m_p-m_q,n_p+n_q}^{\alpha\beta} \\ + s_3^\beta H_{m_p+m_q,n_p-n_q}^{\alpha\beta} + s_4^\beta H_{m_p+m_q,n_p+n_q}^{\alpha\beta} \end{aligned} \tag{8}$$

where for the case of PEC walls the factors s_n^β are given by $s_1^x = s_1^y = 1$; $s_2^x = -1$, $s_2^y = 1$; $s_3^x = 1$, $s_3^y = -1$; $s_4^x = s_4^y = -1$, and for the case with walls made of PMC the sign factors are $s_1^x = s_1^y = 1$; $s_2^x = -1$, $s_2^y = 1$; $s_3^x = -1$, $s_3^y = 1$; $s_4^x = s_4^y = 1$,, where β denotes the source basis function orientation, x or y.

While the above algorithm is directly applicable to the evaluation of the matrix elements in the MoM formulation with geometry conforming to a regular grid, it can also be used for implementation of the MoM with more general off-grid meshes. In this case, taking as basis and testing functions in (2), the delta-functions located at the nodes of the regular grid, i.e.,

$$\begin{aligned} b_q^x(\vec{r}) &= \delta\left[x - \frac{m_q a}{M}\right] \delta\left[y - \frac{n_q b}{N}\right] \\ t_p^x(\vec{r}) &= \delta\left[x - \frac{m_p a}{M}\right] \delta\left[y - \frac{n_p b}{N}\right] \end{aligned}$$

and summation reordering according to [41], we obtain the representation for the Green's function samples on the regular grid in the form of (4)

$$\begin{aligned} G_{pq}^{xx} = & \sum_{m=1}^{M/2-1} \sum_{n=1}^{N/2-1} \sin\frac{n\pi n_p}{N} \sin\frac{n\pi n_q}{N} \cos\frac{m\pi m_p}{M} \\ & \times \cos\frac{m\pi m_q}{M} g_{mn}^{xx}. \end{aligned} \tag{9}$$

By casting (9) into the DFT-based representation similar to (5), we can calculate the Green's function for any pair of observation and source points on the grid as

$$\begin{aligned} G_{pq}^{xx} = \Gamma_{m_p-m_q,n_p-n_q}^{xx} + \Gamma_{m_p-m_q,n_p+n_q}^{xx} + \Gamma_{m_p+m_q,n_p-n_q}^{xx} \\ + \Gamma_{m_p+m_q,n_p+n_q}^{xx} \end{aligned} \tag{10}$$

where the generating matrix Γ^{xx} is defined on the regular grid as $\Gamma^{xx} = \mathrm{FFT}\{g^{xx}\}$ similar to (8). From a matrix of regular grid samples Γ^{xx}, the values of function $\tilde{\Gamma}^{xx}(x,y)$ at any arbitrary location on $x \in [0, 2a]$, $y \in [0, 2b]$ can be obtained via 2-D interpolation [42]. Following a similar procedure for other components of the DGF, we obtain the following continuous dependence of the DGF on the source and observation point coordinates:

$$\begin{aligned} & G^{\alpha\beta}(x,y;x',y') \\ & \quad = s_1^\beta \Gamma^{\alpha\beta}(x-x', y-y') + s_2^\beta \Gamma^{\alpha\beta}(x-x', y+y') \\ & \qquad + s_3^\beta \Gamma^{\alpha\beta}(x+x', y-y') + s_4^\beta \Gamma^{\alpha\beta}(x+x', y+y'). \end{aligned} \tag{11}$$

Formula (11) can be utilized in evaluation of the impedance matrix elements in the MoM defined on nonuniform meshes using standard quadrature rules. Sign factors s in (11) are the same as in (8). The proposed approach is appropriate for evaluation of the matrix elements in pairs of source and basis functions,

which do not encounter the DGF singularity. The matrix elements involving integration of the DGF singularity in the case of a nonuniform mesh-based MoM can be evaluated via direct summation over waveguide modes in (2) after the surface integrals are evaluated analytically. Alternatively, the static component of the DGF can be first extracted from the waveguide DGF spectrum using the discrete complex image method (DCIM) [43], [44] prior to its casting to the form (9). Subsequently, the infinite series of the static contribution can be calculated as described in the Appendix [45].

IV. FFT-Enhanced MSOs of UFFT

A modification of the PFFT algorithm [5] is described for acceleration of the matrix-vector product $\hat{\mathbf{Z}}^{\text{far}} \cdot \mathbf{I}$ in the case of shielded layered media DGF. It is important to point out that the distinction between "near-zone" and "far-zone" interactions in the PFFT algorithm is not based on electrical distance [33]–[35]. Thus, the method can be applied without loss of effectiveness for structures ranging from electrically large to sub-wavelength [35].

First, a regular rectangular grid with discrete increments $\Delta x = a/(K_1 - 1)$ and $\Delta y = b/(K_2 - 1)$, which we refer to as the PFFT grid (as in this work, it may optionally be distinct from the regular grid used in the MFO), is overlain on the rectangle defined by the intervals $x \in [0, 2a]$ and $y \in [0, 2b]$ corresponding to twice the waveguide cross section over x and y. In the following, the indices $k_{1,2} = 0, \ldots, 2(K_{1,2} - 1)$ are used to identify the nodes of the grid. In Fig. 1, a portion of this grid for $k_{1,2} = 0, \ldots, K_{1,2} - 1$ is shown by circles for the case when the structure under study is a six-patch antenna array. Also shown in Fig. 1 is the MoM grid that is used for the discretization of the unknown current density on the patches. It is noted that the MoM mesh can be nonuniform. It is stressed that the PFFT grid is introduced over an area four times that of the original cross section in order for the DGF used in (11) to yield all elements of the periodicity [39] for the $\mathbf{Z}$-matrix elements. Once the PFFT grid is introduced, each of the basis and testing functions $b_i^\alpha(\vec{r})$ and $t_i^\alpha(\vec{r})$ are replaced by M^2 delta sources, thus defining the so-called expansion box (also known as a stencil) [5],

$$\hat{b}_i^\alpha(\vec{r}) = \sum_{k_1=0}^{2(K_1-1)} \sum_{k_2=0}^{2(K_2-1)} B^\alpha_{k_1,k_2,i} \delta\left(x - x^\alpha_{k_1,i}\right) \delta\left(y - y^\alpha_{k_2,i}\right) \tag{12a}$$

$$\hat{t}_i^\alpha(\vec{r}) = \sum_{k_1=0}^{2(K_1-1)} \sum_{k_2=0}^{2(K_2-1)} T^\alpha_{k_1,k_2,i} \delta\left(x - x^\alpha_{k_1,i}\right) \delta\left(y - y^\alpha_{k_2,i}\right). \tag{12b}$$

In the above, $\{x^\alpha_{m_1,i}, y^\alpha_{m_2,i}\}$ are the locations of the delta sources associated with the ith basis or testing function. Even though the indices of summation in (12) run over the entire PFFT grid, only M^2 terms are nonzero for each basis/test function, where M is the order of the expansion box depicted in Fig. 1, which depicts the way the delta-source representation (12) is performed for a basis function in the case of $M = 3$.

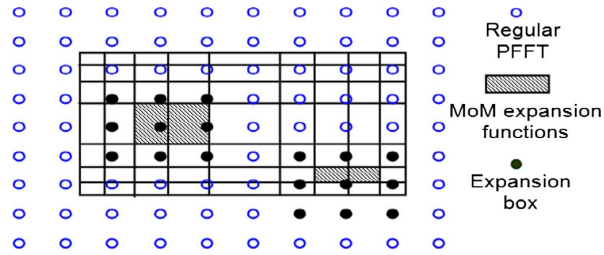

Fig. 1. Projection of the MoM rooftop basis functions on the regular PFFT grid.

Given the order M of the expansion box, M^2 nodes of the PFFT grid are allocated for the assignment of the delta sources. The choice of the expansion coefficients, represented in compact form through the arrays $\mathbf{B}$ and $\mathbf{T}$, is not unique. Various criteria may be used to specify their values. Investigation shows that even though the multipole reproduction criteria of [5] traditionally used in PFFT for open structures provides sufficient accuracy, more specific criteria based on the least squares approximation of the fields of the waveguide eigenmodes can provide better accuracy. One may consider the expression for the β component of field produced by jth expansion function $b_j^\beta(\vec{r})$,

$$E_j^{\alpha\beta}(\vec{r}) = \sum_{m=0}^{\infty} \sum_{n=0}^{\infty} f^\alpha_{mn} \beta \varphi^\alpha_{mn}(\vec{r}) \int_{S_j} b_j^\beta(\vec{r}') \varphi^\beta_{mn}(\vec{r}') ds'. \tag{13}$$

It appears that $b_j^\beta(\vec{r})$ should be replaced with an approximation,$\hat{b}_j^\beta(\vec{r})$, the error in the scattered field produced by the jth expansion function is given by the functional, Θ,

$$\Theta_{m,n,j} = \int_{S_j} \left(b_j^\beta(\vec{r}') - \hat{b}_j^\beta(\vec{r}') \right) \varphi^\beta_{mn}(\vec{r}') ds' \tag{14}$$

for $m = 0, \ldots, \infty$ and $n = 0, \ldots, \infty$. Hence, the problem of projecting the jth expansion function on the PFFT grid can be formulated as the problem of minimization of the functional (14) in the least squares sense [39] as follows:

$$\text{minimize over } B^\beta_{k_1,k_2,j} : \sum_{m=0}^{\mu} \sum_{n=0}^{\nu} \Theta^2_{m,n,j} \tag{15}$$

where μ and ν are truncation indices that must be chosen such that all eigenmodes that are excited appreciably by the specific expansion function are taken into account. One can show [39] that minimization of (15) is equivalent to the solution of the following redundant set of $\mu\nu$ linear algebraic equations with M^2 unknowns $B^\beta_{m_1,m_2,j}$:

$$\sum_{m_1=1}^{M} \sum_{m_2=1}^{M} \varphi^\beta_{mn}\left(x^\beta_{m_1,j}, y^\beta_{m_2,j}\right) B^\beta_{m_1,m_2,j} = \int_{S_j} \varphi^\beta_{mn}(\vec{r}) b_j^\beta(\vec{r}) ds \tag{16}$$

where $m = 0, \ldots, \mu, n = 0, \ldots, \nu$. The indices $m_{1,2}$ are used in (16) instead of $k_{1,2}$ to single out the M_2 nonzero elements $B^\beta_{m_1,m_2,j}$ from the elements $B^\beta_{k_1,k_2,j}$ of the entire array, where $k_{1,2} = 0, \ldots, 2(K_{1,2} - 1)$. The procedure for defining the coefficients of the projection of a testing function on the PFFT grid is the same as the one for the expansion functions.

Once the coefficients of the arrays $\mathbf{B}$ and $\mathbf{T}$ have been determined, substitution of (12) into the integrals in (2) yields the following expressions for the matrix-vector product $\hat{\mathbf{Z}} \cdot \mathbf{I}$:

$$\begin{aligned}\hat{\mathbf{Z}} \cdot \mathbf{I} &= \sum_{j=1}^{N^\beta} \hat{Z}_{ij}^{\alpha\beta} I_j^\beta \\ &= \sum_{k_1=0}^{2(K_1-1)} \sum_{k_2=0}^{2(K_2-1)} T_{k_1,k_2,i}^{\alpha} \\ &\quad \times \sum_{k_1'=0}^{2(K_1-1)} \sum_{k_2'=0}^{2(K_2-1)} G^{\alpha\beta}\left(k_1\Delta x, k_2\Delta y; k_1'\Delta x, k_2'\Delta y\right) \\ &\quad \times \sum_{j=1}^{N^\beta} I_j^\beta B_{k_1',k_2',j}^{\beta} \end{aligned} \tag{17}$$

where $i = 1, 2, \ldots, N^\alpha$. Substitution of (11) into (17) with the well-known MoM procedure yields the convolution-correlation representation for the matrix-vector product $\hat{\mathbf{Z}} \cdot \mathbf{I}$, shown in (18) at the bottom of this page, where the matrix $\Lambda_{k_1',k_2'}^{\beta}$ is defined in terms of the product

$$\Lambda_{k_1',k_2'}^{\beta} = \sum_{j=1}^{N^\beta} B_{k_1',k_2',j}^{\beta} I_j^\beta. \tag{19}$$

In matrix form,

$$\begin{aligned}&\hat{\mathbf{Z}} \cdot \mathbf{I} \\ &= \begin{bmatrix} \mathbf{T}^x \cdot \mathbf{G}^{xx} \cdot \left(\mathbf{B}^x\right)^T \cdot \mathbf{I}^x + \mathbf{T}^x \cdot \mathbf{G}^{xy} \cdot \left(\mathbf{B}^y\right)^T \cdot \mathbf{I}^y \\ \mathbf{T}^y \cdot \mathbf{G}^{yx} \cdot \left(\mathbf{B}^x\right)^T \cdot \mathbf{I}^x + \mathbf{T}^y \cdot \mathbf{G}^{yy} \cdot \left(\mathbf{B}^y\right)^T \cdot \mathbf{I}^y \end{bmatrix} \\ &= \begin{bmatrix} \mathbf{T}^x \cdot \left(\sum_{n=1}^4 s_n^{xx} \Gamma_n^{xx} \cdot \left(\hat{\Lambda}^x\right)^T + \sum_{n=1}^4 s_n^{xy} \Gamma_n^{xy} \cdot \left(\hat{\Lambda}^y\right)^T \right) \\ \mathbf{T}^y \cdot \left(\sum_{n=1}^4 s_n^{yx} \Gamma_n^{yx} \cdot \left(\hat{\Lambda}^x\right)^T + \sum_{n=1}^4 s_n^{yy} \Gamma_n^{yy} \cdot \left(\hat{\Lambda}^y\right)^T \right) \end{bmatrix} \end{aligned} \tag{20}$$

where $\Gamma_n^{\alpha\beta}, n = 1, \ldots, 4$, denote the Toeplitz and Hankel matrices formed by the four convolution-correlation terms entering in (20), and the superscript T stands for matrix transpose. Each partial matrix-vector product $\Gamma_n^{\alpha\beta} \cdot \left(\hat{\Lambda}^\beta\right)^T$ can be computed using the FFT algorithm [39], thus providing the desired $O(N \log N)$ complexity for the MSO

$$\Gamma_n^{\alpha\beta} \cdot \left(\hat{\Lambda}^\beta\right)^T = \mathrm{FFT}_n^{-1}\left\{\mathrm{FFT}_n\left\{\Gamma_n^{\alpha\beta}\right\} \cdot \mathrm{FFT}_n\left\{\left(\hat{\Lambda}^\beta\right)^T\right\}\right\}$$

where $\mathrm{FFT}_n\{\ldots\}$ and $\mathrm{FFT}_n^{-1}\{\ldots\}$ are operations of the forward and inverse DFT, respectively. The index n has been assigned to the FFT operations because in the case when the matrix-vector product $\Gamma_n^{\alpha\beta} \cdot \left(\hat{\Lambda}^\beta\right)^T$ contains correlation dependence over a certain index, in addition to the forward FFT operation one has to perform a certain rearrangement of the elements in the spectral domain with respect to that index [39].

Since the FFTs of the DGF matrices $\mathrm{FFT}_n\{\Gamma_n^{\alpha\beta}\}$ are computed once and then stored, it is straightforward to show that, for an iterative matrix solution with number of iterations N_{iter}, the number of required operations scales as $4N_{iter}\alpha N \log N$, where $\alpha N \log N$ is the time per FFT operation. At each iteration, the above process calculates the product $\hat{\mathbf{Z}} \cdot \mathbf{I}$ [see (3)]. While the calculation of the "far-zone" interactions using the PFFT process are reasonably accurate, the calculated "near-zone" interactions are not. Thus, the operation $\hat{\mathbf{Z}} \cdot \mathbf{I} - \mathbf{Z}_{\mathrm{near}} \cdot \mathbf{I}$ is required to correct the calculation of the "near-zone" interactions by replacing the PFFT calculated ones with those obtained using the exact MoM representation of the expansion function interactions [see (8)]. These operations are of $O(N)$complexity. In addition to reduction in the computational complexity of iterative solutions, PFFT implementation relaxes memory requirements.

Since only the "near-zone" matrix elements are stored, the $O(N^2)$ overhead associated with the storage of the MoM matrix is avoided. Instead, storing of the "near-zone" interactions results in memory requirements that scale as $O(N)$ with aggressive near part sizing. However, one can increase the size of the near part to provide better convergence behavior, essentially trading memory capacity for CPU time, and potentially, accuracy. Furthermore, due to the Toeplitz/Hankel-like characteristics [39] of the Green's function matrices $\Gamma^{\alpha\beta}$ on the PFFT grid, those memory requirements scale similarly as $O(N_b M_b)$.

$$\begin{aligned}\hat{\mathbf{Z}} \cdot \mathbf{I} = \sum_{k_1=0}^{2(K_1-1)} \sum_{k_2=0}^{2(K_2-1)} T_{k_1,k_2,i}^{\alpha} \Bigg\{ & s_1^\beta \sum_{k_1'=0}^{2(K_1-1)} \sum_{k_2'=0}^{2(K_2-1)} \Gamma^{\alpha\beta}\left[\left(k_1-k_1'\right)\Delta x, \left(k_2-k_2'\right)\Delta y\right] \Lambda_{k_1',k_2'}^{\beta} \\ & + s_2^\beta \sum_{k_1'=0}^{2(K_1-1)} \sum_{k_2'=0}^{2(K_2-1)} \Gamma^{\alpha\beta}\left[\left(k_1-k_1'\right)\Delta x, \left(k_2+k_2'\right)\Delta y\right] \Lambda_{k_1',k_2'}^{\beta} \\ & + s_3^\beta \sum_{k_1'=0}^{2(K_1-1)} \sum_{k_2'=0}^{2(K_2-1)} \Gamma^{\alpha\beta}\left[\left(k_1+k_1'\right)\Delta x, \left(k_2-k_2'\right)\Delta y\right] \Lambda_{k_1',k_2'}^{\beta} \\ & + s_4^\beta \sum_{k_1'=0}^{2(K_1-1)} \sum_{k_2'=0}^{2(K_2-1)} \Gamma^{\alpha\beta}\left[\left(k_1+k_1'\right)\Delta x, \left(k_2+k_2'\right)\Delta y\right] \Lambda_{k_1',k_2'}^{\beta} \Bigg\} \end{aligned} \tag{18}$$

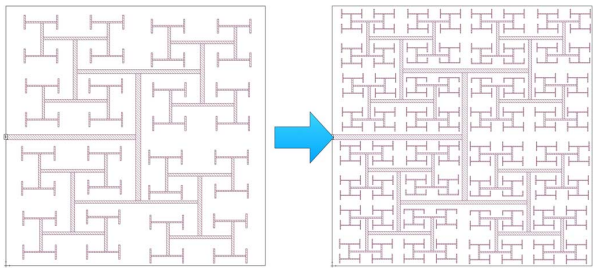

Fig. 2. Fractal nature of clock networks allow for scaling the number of unknowns in simulation of an applicable example.

For the benefits of PFFT to be meaningful, the "far-zone" interactions need to be calculated with sufficient accuracy. This, in turn, is dependent on the accuracy of the equivalence from the projection defined in (12).

V. Numerical Results and Discussion

To demonstrate the performance of the proposed UFFT scheme for shielded structures, three examples are considered. For parity, all examples are analyzed on a square microstrip substrate with $\varepsilon_r = 4$.

A. Clock Network Example

An example is developed that is easily scalable with regard to unknowns for demonstration of scaling effects on a common geometry. A digital clock network is chosen (expanding [46]) as it is a fractal geometry for which scaling of N is readily observed by extending the depth of the fractal as in Fig. 2. The example is tested with six different geometries, each with successively more fractal elements, scaling from $N = 4\,190$ to $N = 50\,658$ (Sonnet) and from $N = 4\,190$ to $N = 126\,281$ (UFFT). All examples are analyzed on a 1 cm^2 (5/32 in^2) square substrate at 100 GHz. Note that number of unknowns in conventional Sonnet is limited by the 32-GB memory capacity of the test system. Timing and memory usage are benchmarked against conventional Sonnet for each example possible. Additionally, accuracy is compared in the form of Y-parameters and also calculated current distributions.

All results for this example are computed on the inexpensive Intel core i5-3570k 3.4-GHz quad-core CPU, and can be seen in Fig. 3. The UFFT demonstrates substantial performance benefits over conventional Sonnet both in terms of memory utilization and CPU time. Moreover, while Sonnet is able to take advantage of all CPU cores, multi-threading is left to future work for the UFFT, meaning optimized code will see further performance increases. In a similar fashion to the first example, the overhead of the PFFT algorithm results in circuits featuring a small number of unknowns being computed faster in traditional Sonnet. This takeover occurs when unknowns surpass around 7000.

Accuracy in this example is compared to conventional Sonnet by way of Y-parameters and current distributions. Generally, switching to the PFFT from conventional Sonnet yields an additional 1%–3% error component for dominant Y-parameters in multiport circuits.

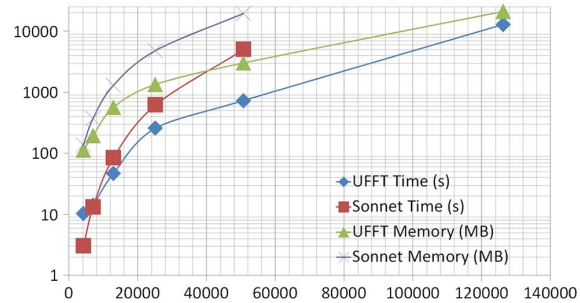

Fig. 3. Performance comparison between UFFT and Sonnet for complete solution of the problem. Memory requirements and solve time are shown. Note that Sonnet curves stop at $N = 50\,658$ due to memory capacity limitations.

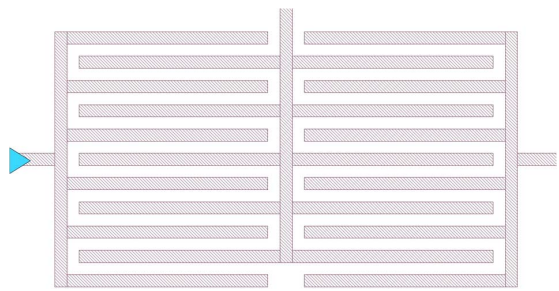

Fig. 4. Interdigital capacitor example circuit geometry. Port excitation is 1 V at the blue triangle (in online version).

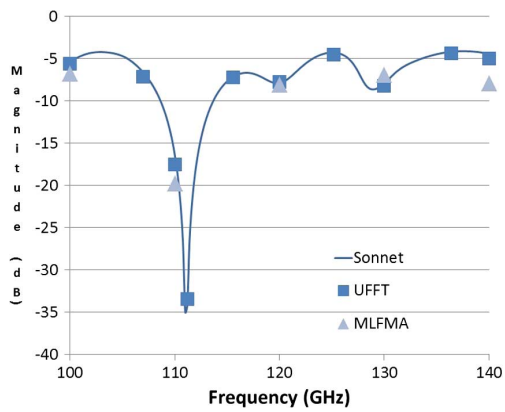

Fig. 5. S11 versus frequency, Sonnet (dark blue line in online version) versus UFFT (medium blue square in online version), versus MLFMA (light blue triangle in online version).

B. Interdigital Capacitor Example

The capacitance of an interdigitated filter is extracted to benchmark accuracy of the UFFT solver, as well as to compare performance versus a state-of-the-art MLFMA algorithm [48]. The example circuit is a microstrip configuration containing three terminals for two capacitors for device loading, following general principles established in [47], and is shown in Fig. 4. The structure is on a 1-cm^2 (5/32 in^2) square micostrip substrate of thickness 0.1 mm (0.004 in) and is simulated at 100 GHz. All fingers are 3.55-mm (0.140 in) long and 0.2-mm (0.008 in) wide. The structure is centered on the substrate with feed lines to the edges. All other lines and gaps are also 0.2 mm (0.008 in) wide with their length being deterministic based on other defined parameters. S-parameters are seen in Fig. 5, and timing is shown in Fig. 6. Note that while the UFFT and Sonnet solvers share partial data from MFOs, the methodology, code, results, required resources, and even language used for coding are distinct between the two. The MFO times in Fig. 6

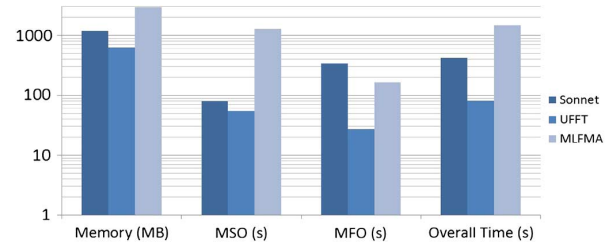

Fig. 6. Logarithmic timing data for MSO, MFO, and overall time, as well as memory usage for Sonnet, UFFT, and MLFMA simulations of the interdigital capacitor geometry.

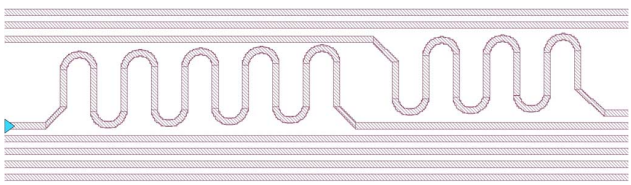

Fig. 7. Geometry for the digital delay line (meander) example. Port excitation is 1 V at the blue triangle (in online version).

are measured as longer than would be seen in practice due to prototype-mandated diagnostics. As they are uniformly increased as a percentage, times are valid for comparison. Note that the performance of the UFFT algorithm exceeds MLFMA in a large part due to the 3-D planar nature of the UFFT implementation versus the arbitrary 3-D implementation of the MLFMA algorithm used [48]. Simply, the UFFT has more efficient meshing of the structure. This is because only the conductor needs to be surface meshed in the UFFT while the entire substrate needs to be volume meshed in the MLFMA. This results in $N = 12\,491$ for UFFT versus $N = 97\,944$ for the MLFMA.

C. Digital Bus With Delay Line

A digital bus with a meander delay line example is used to demonstrate the accuracy of the UFFT solver for circuits featuring curved metallization. The example geometry, shown in Fig. 7, consists of $N = 26\,286$ unknowns modeling an 8-bit bus printed in a microstrip configuration on a 10 cm $\times$ 10 cm $\times$ 1 mm (3.94 in $\times$ 3.94 in $\times$ 0.039 in) substrate. The bus features lines with width and separation of 1 mm (0.039 in), two of which have delays of separate amounts. The meander geometry is of interest as it demonstrates the capability of the solver to accurately model rounded surfaces despite being discretized solely by rectangular basis functions.

Results of current distribution behavior, shown in Fig. 8 with excitation of the upper delay line, are very good. Plots show accurate physical behavior in terms of full-wave patterns, edge singularities, and other physical phenomenon. The figure compares Sonnet (*top*), the UFFT (*middle*), and the difference between the two (*bottom*).

As seen in Fig. 9, simulation timing and memory requirements again heavily favor the UFFT versus conventional Sonnet, despite the single-threaded implementation for the UFFT and multi-threaded implementation for Sonnet. Note that both MFO times include file write times as in the previous example.

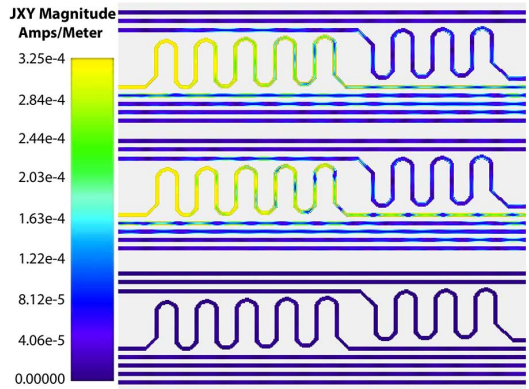

Fig. 8. Current distributions as calculated by Sonnet (*top*) and UFFT (*middle*), and the difference between the two (*bottom*).

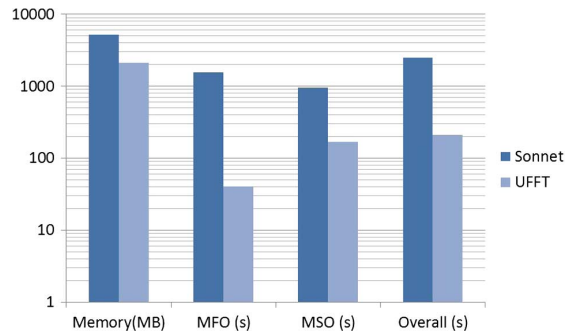

Fig. 9. Memory requirements, MFO time, and MSO time for Sonnet and UFFT for the meander example.

VI. Conclusion

This work has introduced a new methodology, UFFT, which combines FFT-enhanced MFOs with FFT-enhanced MSOs in MoM analysis of planar circuits embedded in layered media inside a rectangular enclosure. The UFFT framework features a modified version of Sonnet's FFT-based MFO combined with a precorrected-FFT acceleration of the MSO, and identifies, develops, tests, and shows a meaningful relationship between the two. Further, FFT-enhanced MFO as in [38] is detailed for the first time. Indeed, the underlying principles of the UFFT can be applied to a broad range of workflows and applications. Such implementations become inevitable when the number of unknowns associated with electromagnetic analysis becomes high, as in conventional RF integrated circuit (RFIC) design.

CPU scaling of $O(N \log N)$ and memory scaling of $O(N)$ are demonstrated with a number of large examples, with tremendous performance improvements shown versus the traditional MoM implementation in Sonnet with identical meshing. Moreover, even larger performance improvements are shown versus a state-of-the-art MLFMA implementation due to more efficient meshing of the structure.

Appendix

Evaluation of Green's Function Samples via DCIM Fitting and Ewald's Transform

For evaluation of the near interactions between elements nonconformal to the uniform grid, the approach based on subtraction and analytic integration of the $1/r$ Green's function singu-

larity followed by quadrature-based integration [49] of the nonsingular part of the DGF is commonly used [33]–[35].

First, the components $G^{\alpha\beta}$ are expressed in terms of the scalar potentials [50] as in

$$G^{xx} = \frac{\partial^2 F_x^{\mathrm{TM}}}{\partial x^2} - k^2 \frac{\partial^2 F_x^{\mathrm{TE}}}{\partial y^2} \tag{21}$$

where k is the wavenumber of the media at the observation point. The scalar potentials $F_\beta^{\mathrm{TM,TE}}$ are the contributions to the total field. Their spatial dependence has the form

$$\begin{aligned} F_\beta^{\mathrm{TE,TM}}&(x,y;x',y') \\ &= s_1^\beta \Phi^{\mathrm{TE,TM}}(x-x',y-y') + s_2^\beta \Phi^{\mathrm{TE,TM}}(x-x',y+y') \\ &\quad + s_3^\beta \Phi^{\mathrm{TE,TM}}(x+x',y-y') + s_4^\beta \Phi^{\mathrm{TE,TM}}(x+x',y+y') \end{aligned} \tag{22}$$

where sign factors are as shown in (8) and potential $\Phi^{\mathrm{TE,TM}}$ is

$$\Phi^{\mathrm{TE,TM}}(\xi,\eta) = \frac{-W_0 i}{8ab}\frac{1}{k}\sum_{m=-\infty}^{\infty}\sum_{n=-\infty}^{\infty}\frac{\varphi_{mn}^{\mathrm{TE,TM}}}{k_{mn}} e^{ik_x\xi + ik_y\eta}. \tag{23}$$

In (23), $\varphi_{mn}^{\mathrm{TE,TM}}$ is dimensionless and defined by the layered media and waveguide. Consider the case where the media consist of a single layer of thickness l and of relative permittivity ε. Let the 1 denote free space and 2 dielectric,

$$\varphi_{mn}^{\mathrm{TE}} = \frac{1}{i\gamma_{mn}^{(1)} k_{mn}}\left[1 + R_{mn}^{\mathrm{TE}}\right] \tag{24a}$$

$$\varphi_{mn}^{\mathrm{TM}} = \frac{i\gamma_{mn}^{(1)}}{k_{mn}}\left[1 + R_{mn}^{\mathrm{TM}}\right] \tag{24b}$$

where

$$\gamma_{mn}^{(j)} = \begin{cases} \sqrt{k_0^2\varepsilon_j - k_{mn}^2}, & \text{if } k_0^2\varepsilon_j \geq k_{mn}^2 \\ -i\sqrt{k_{mn}^2 - k_0^2\varepsilon_j}, & \text{if } k_0^2\varepsilon_j < k_{mn}^2 \end{cases}$$

is the propagation constant of the mnth mode inside the jth domain, $j = 1, 2$. In (24), it is assumed that the source and observation points have the same location, $z = z' = 0$, corresponding to the plane located above the air–dielectric interface. The reflection coefficients in (24a) and (24b) for this single layer configuration are

$$R_{mn}^{\mathrm{TE}} = \frac{\left[\left(\gamma_{mn}^{(1)}\right)^2 - \left(\gamma_{mn}^{(2)}\right)^2\right] i\tan\left(l\gamma_{mn}^{(2)}\right)}{2\gamma_{mn}^{(1)}\gamma_{mn}^{(2)} + \left[\left(\gamma_{mn}^{(1)}\right)^2 + \left(\gamma_{mn}^{(2)}\right)^2\right] i\tan\left(l\gamma_{mn}^{(2)}\right)} \tag{25a}$$

$$R_{mn}^{\mathrm{TM}} = \frac{\left[\left(\gamma_{mn}^{(2)}\right)^2 - \varepsilon_2^2\left(\gamma_{mn}^{(1)}\right)^2\right] i\tan\left(l\gamma_{mn}^{(2)}\right)}{2\varepsilon_2\gamma_{mn}^{(1)}\gamma_{mn}^{(2)} + \left[\left(\gamma_{mn}^{(2)}\right)^2 + \varepsilon_2^2\left(\gamma_{mn}^{(1)}\right)^2\right] i\tan\left(l\gamma_{mn}^{(2)}\right)}. \tag{25b}$$

The key to the acceleration of the series in (23) is the fitting of the spectra $\varphi_{mn}^{\mathrm{TE,TM}}$ as a function of k_{mn} by exponentials, making use of the generalized pencil-of-function technique (GPOF) [51]. Herewith, the fitting is performed for such $k_{mn} > K$ that the spectra $\varphi_{mn}^{\mathrm{TE,TM}}$ are purely real. Hence, it is

$$\begin{aligned} \varphi_{mn}^{\mathrm{TE,TM}} &\simeq \hat{\varphi}_{mn}^{\mathrm{TE,TM}} \\ &= \sum_{p=1}^{P} u_p^{\mathrm{TE,TM}} \exp\left(-\zeta_p^{\mathrm{TE,TM}} k_{mn}\right), k_{mn} \in [K, \infty] \end{aligned} \tag{26}$$

where all constants, $\zeta_p^{\mathrm{TE,TM}}$, $p = 1, \ldots, P$ in (26) are positive real. The series in (23) with the approximate spectra $\hat{\varphi}_{mn}^{\mathrm{TE,TM}}$ can then be taken as the reference series for the application of Kummer's transformation [52]. Thus, (23) is computed as

$$\begin{aligned} \Phi^{\mathrm{TE,TM}}&(\xi,\eta) \\ &= \frac{-W_0 i}{8ab}\frac{1}{k}\left[\sum_{m=-\infty}^{\infty}\sum_{n=-\infty}^{\infty}\left(\varphi_{mn}^{\mathrm{TE,TM}} - \hat{\varphi}_{mn}^{\mathrm{TE,TM}}\right)\cdot\frac{e^{ik_x\xi + ik_y\eta}}{k_{mn}}\right. \\ &\quad + \sum_{p=1}^{P} u_p^{\mathrm{TE,TM}} \sum_{m=-\infty}^{\infty}\sum_{n=-\infty}^{\infty}\frac{e^{-\zeta_p^{\mathrm{TE,TM}} k_{mn}}}{k_{mn}} \\ &\quad \left. \times e^{ik_x\xi + ik_y\eta}\right]. \end{aligned} \tag{27}$$

In the above expression, the series containing the difference $(\varphi_{mn}^{\mathrm{TE,TM}} - \hat{\varphi}_{mn}^{\mathrm{TE,TM}})$ converges very fast as soon as the indices m and n assume values such that $k_{mn} > K$. The second term is first reduced to the free-space periodic DGF using Poisson summation formula [49], [53]

$$\begin{aligned} &\frac{1}{4ab}\sum_{m=-\infty}^{\infty}\sum_{n=-\infty}^{\infty} e^{\frac{-\zeta_p^{\mathrm{TE,TM}} k_{mn}}{k_{mn}}} e^{ik_x\xi + ik_y\eta} \\ &= \frac{1}{2\pi}\sum_{m=-\infty}^{\infty}\sum_{n=-\infty}^{\infty}\frac{1}{\sqrt{(\xi+2ma)^2 + (\eta+2nb)^2 + \left(\zeta_p^{\mathrm{TE,TM}}\right)^2}}. \end{aligned} \tag{28}$$

The series in the right-hand side of (28) can be evaluated using Ewald's technique yielding exponential convergence [54].

REFERENCES

[1] C. F. Smith, A. F. Peterson, and R. Mittra, "The biconjugate gradient method for electromagnetic scattering," *IEEE Trans. Antennas Propag.*, vol. 38, no. 6, pp. 938–940, Jun. 1990.

[2] R. Coifman, V. Rokhlin, and S. Wandzura, "The fast multipole method for the wave equation: A pedestrian prescription," *IEEE Antennas Propagat. Mag.*, vol. 35, no. 3, pp. 7–12, Jun. 1993.

[3] *Fast and Efficient Algorithms in Computational Electromagnetics*, W. C. Chew, J.-M. Jin, E. Michielssen, and J. Song, Eds. Norwood, MA, USA: Artech House, 2001.

[4] E. Bleszynski, M. Bleszynski, and T. Jaroszewicz, "A fast integral-equation solver for electromagnetic scattering problems," in *IEEE AP-S Int. Antennas Propag. Symp. Dig.*, Seattle, WA, USA, Jun. 20–24, 1994, vol. 1, pp. 416–419.

[5] E. Bleszynski, M. Bleszynski, and T. Jaroszewicz, "AIM: Adaptive integral method for solving large-scale electromagnetic scattering and radiation problems," *Radio Sci.*, vol. 31, no. 5, pp. 1225–1251, Sep. –Oct. 1996.

[6] A. Zhu and S. D. Gedney, "A quadrature-sampled precorrected FFT method for the electromagnetic scattering from inhomogeneous objects," *Antennas Wireless Propag. Lett.*, vol. 2, no. 1, pp. 50–53, 2003.

[7] A. E. Yilmaz, J.-M. Jin, and E. Michielssen, "Time domain adaptive integral method for surface integral equations," *IEEE Trans. Antennas Propag.*, vol. 52, no. 10, pp. 2692–2708, Oct. 2004.

[8] A. E. Yilmaz, "A two-scale AIM for fast solution of volume integral equations," in *Proc. Appl. Comput. Electromagn. Soc. Conf.*, Monterey, CA, USA, Mar. 2009, pp. 511–516.

[9] F. Ling, C.-F. Wang, and J.-M. Jin, "An efficient algorithm for analyzing large-scale microstrip structures using adaptive integral method combined with discrete complex image method," *IEEE Trans. Microw. Theory Techn.*, vol. 48, no. 5, pp. 832–839, May 2000.

[10] N. Yuan, T. S. Yeo, X.-C. Nie, Y.-B. Gan, and L.-W. Li, "Analysis of probe-fed conformal microstrip antennas on finite grounded substrate," *IEEE Trans. Antennas Propag.*, vol. 54, no. 2, pp. 554–563, Feb. 2006.

[11] N. N. Bojarski, "K-space formulation of the electromagnetic scattering problems," Air Force Avion. Lab., Wright-Patterson Air Force Base, OH, USA, Techn. Rep. AFAL-TR-71-75, Mar. 1971.

[12] M. F. Catedra, R. F. Torres, J. Basterrechea, and E. Gago, *The CG-FFT Method—Application of Signal Processing Techniques to Electromagnetics*. Norwood, MA, USA: Artech House, 1995.

[13] J. D. Morsey, V. I. Okhmatovski, and A. C. Cangellaris, "Finite-thickness conductor models for full-wave analysis of interconnects with a fast integral equation method," *IEEE Adv. Packag.*, vol. 27, no. 1, pp. 24–33, Feb. 2004.

[14] C.-F. Wang, F. Ling, and J.-M. Jin, "A fast full-wave analysis of scattering and radiation from large finite arrays of microstrip antennas," *IEEE Trans. Antennas Propag.*, vol. 46, no. 10, pp. 1467–1474, Oct. 1998.

[15] S. M. Seo, C.-F. Wang, and J.-F. Lee, "Analyzing PEC scattering structures using an IE-FFT algorithm," *Appl. Comput. Electromagn. Soc. J.*, vol. 24, no. 2, pp. 116–128, 2009.

[16] S.-Q. Li, Y.-X. Yu, K. F. Chan, C. H. Chan, and L. Tsang, "A sparse-matrix/canonical grid method for analyzing densely packed interconnects," *IEEE Trans. Microw. Theory Techn.*, vol. 49, no. 7, pp. 1221–1228, Jul. 2001.

[17] S. Kapur and D. E. Long, "IES/sup 3/: A fast integral equation solver for efficient 3-dimensional extraction," in *Proc. IEEE/ACM Int. Comput.-Aided Design Conf.*, Washington, DC, USA, Nov. 9–13, 1997, pp. 448–455.

[18] D. Gope and V. Jandhyala, "Pilot: A fast algorithm for enhanced 3-D parasitic capacitance extraction efficiency," in *Elect. Perform. Elect. Packag. Dig.*, Princeton, NJ, USA, Oct. 27–29, 2003, pp. 337–340.

[19] D. Gope and V. Jandhyala, "Efficient solution of EFIE via low-compression of multilevel predetermined interactions," *IEEE Trans. Antennas Propag.*, vol. 53, no. 10, pp. 3324–3333, Oct. 2005.

[20] W. Hackbusch, "A sparse matrix arithmetic based on H-matrices. Part I: Introduction to H-matrices," *Computing*, vol. 62, no. 2, pp. 89–108, 1999.

[21] S. Borm, *Efficient Numerical Methods for Non-local Operators: H2-Matrix Compression, Algorithms, Analysis*. Zürich, Switzerland: European Math. Soc., 2010.

[22] W. Chai and D. Jiao, "A linear-complexity direct integral equation solver accelerated by a new rank-minimized H2-representation for large-scale 3-D interconnect extraction," in *IEEE MTT-S Int. Microw. Symp. Dig.*, Montreal, QC, Canada, Jun. 2012, pp. 1–3.

[23] J. Ostrowski, Z. Andjelic, M. Bebendorf, B. Cranganu-Cretu, and J. Smajic, "Fast BEM-solution of Laplace problems with H-matrices and ACA," *IEEE Trans. Magn.*, vol. 42, no. 4, pp. 627–630, Apr. 2006.

[24] K. Zhao, M. N. Vouvakis, and J.-F. Lee, "The adaptive cross approximation algorithm for accelerated method of moments computations of EMC problems," *IEEE Trans. Electromagn. Compat.*, vol. 47, no. 4, pp. 763–773, Nov. 2005.

[25] W. C. Chew, J.-M. Jin, C.-C. Lu, E. Michielssen, and J. M. Song, "Fast solution methods in electromagnetics," *IEEE Trans. Antennas Propag.*, vol. 45, no. 3, pp. 533–543, Mar. 1997.

[26] W. Chai and D. Jiao, "A complexity-reduced H-matrix based direct integral equation solver with prescribed accuracy for large-scale electrodynamic analysis," in *IEEE Int. Antennas Propag. Symp.*, Jul. 2010, pp. 1–4.

[27] L. Jiang, "Studies on low frequency fast multipole algorithms," Ph.D. dissertation, Dept. Elect. Comput. Eng., Univ. Illinois at Urbana-Champaign, Champaign, IL, USA, 2004.

[28] B. Hu and W. C. Chew, "Fast inhomogeneous plane wave algorithm for 3-D buried object problems," in *Proc. IEEE Antennas Propag. Soc. Int. Symp.*, San Antonio, TX, USA, Jun. 2002, vol. 3, pp. 560–563.

[29] V. Jandhyala, E. Michielssen, and R. Mittra, "A memory-efficient, adaptive algorithm for multipole-accelerated capacitance computation in a stratified dielectric medium," *Int. J. Microw. Millimeter-Wave Comput.-Aided Eng.*, vol. 6, no. 6, pp. 381–390, 1996.

[30] Y. C. Pan and W. C. Chew, "A hierarchical fast-multipole method for stratified media," *Microw. Opt. Technol. Lett.*, vol. 27, no. 1, pp. 13–17, 2000.

[31] V. Rokhlin and S. Wandzura, "The fast multipole method for periodic structures," in *IEEE AP-S Int. Symp. Dig.*, Seattle, WA, USA, Jun. 20–24, 1994, vol. 1, pp. 424–426.

[32] T. J. Cui and W. C. Chew, "Fast algorithm for electromagnetic scattering by buried 3-D dielectric objects of large size," *IEEE Trans. Geosci. Remote Sens.*, vol. 37, no. 5, pp. 2597–2608, Sep. 1999.

[33] *Fast and Efficient Algorithms in Computational Electromagnetics*, W. C. Chew, J. M. Jin, E. Michielssen, and J. Song, Eds. Norwood, MA, USA: Artech House, 2001, pp. 729–772.

[34] V. Okhmatovski, J. D. Morsey, and A. C. Cangellaris, "Loop-tree implementation of the adaptive integral method for numerically stable broadband fast electromagnetic modeling," *IEEE Trans. Antennas Propag.*, vol. 52, no. 8, pp. 2130–2140, Aug. 2004.

[35] V. Okhmatovski, M. Yuan, I. Jeffrey, and R. Phelps, "A three-dimensional precorrected FFT algorithm for fast method of moments solutions of the mixed-potential integral equation in layered media," *IEEE Trans. Microw. Theory Techn.*, vol. 57, no. 12, pp. 3505–3517, Dec. 2009.

[36] K. Yang and A. E. Yilmaz, "A three-dimensional adaptive integral method for scattering from structures embedded in layred media," *IEEE Trans. Geosci. Remote Sens.*, vol. 50, no. 4, pp. 1130–1139, Apr. 2012.

[37] V. I. Okhmatovski and A. C. Cangellaris, "Fast electromagnetic analysis of dense shielded integrated circuits using the adaptive integral method (AIM)," in *IEEE MTT-S Int. Microw. Symp. Dig.*, Phoenix, AZ, USA, May 2001, vol. 3, pp. 1929–1932.

[38] *"The Sonnet Suite User's Manual,"* Sonnet Softw. Inc., North Syracuse, NY, USA, 2013.

[39] W. Press, S. Teukolsky, W. Vetterling, and B. Flannery, *Numerical Recipes in Fortran 77*. Cambridge, U.K.: Cambridge Univ. Press, 1999.

[40] G. V. Eleftheriades, J. R. Mosig, and M. Guglielmi, "A fast integral equation technique for shielded planar circuits defined on nonuniform meshes," *IEEE Trans. Microw. Theory Techn.*, vol. 44, no. 12, pp. 2293–2296, Dec. 1996.

[41] J. Rautio, "A time–harmonic electromagnetic analysis of shielded microstrip circuits," Ph.D. dissertation, Elect. Comput. Eng. Dept., Syracuse Univ., Syracuse, NY, USA, 1986.

[42] M. Abramovitz and I. A. Stegun, *Handbook of Mathematical Functions*. New York, NY, USA: Dover, 1965.

[43] Y. L. Chow, J. J. Yang, D. G. Fang, and G. E. Howard, "A closed-form spatial Green's function for the thick microstrip substrate," *IEEE Trans. Microw. Theory Techn.*, vol. 39, no. 3, pp. 588–592, Mar. 1991.

[44] A. Alparslan, M. I. Aksun, and K. A. Michalski, "Closed-form Green's functions in planar layered media for all ranges and materials," *IEEE Trans. Microw. Theory Techn.*, vol. 58, no. 3, pp. 602–613, Mar. 2010.

[45] D. R. Wilton, S. M. Rao, A. W. Glisson, D. H. Schaubert, O. Al-Bundak, and C. M. Butler, "Potential integrals for uniform and linear source distributions on polygonal and polyhedral domains," *IEEE Trans. Antennas Propag.*, vol. MTT-32, no. 3, pp. 276–281, Mar. 1984.

[46] B. J. Rautio, V. I. Okhmatovski, and J. K. Lee, "Fast 3-D planar electromagnetic analysis via unified-FFT method," in *IEEE MTT-S Int. Microw. Symp. Dig.*, Seattle, WA, USA, Jun. 2–7, 2013, pp. 1–3.

[47] N. Miyazawa, "Device having interdigital capacitor," U.S. Patent 6 949 811, Sep. 27, 2005.

[48] *"Wave3D CAD Manual,"* CEMWorks, Scottsdale, AZ, USA, 2013.

[49] A. F. Peterson, S. L. Ray, and R. Mittra, *Computational Methods for Electromagnetics*. Piscataway, NJ, USA: IEEE Press, 1998.

[50] J. R. Wait, *Electromagnetic Wave Theory*. New York, NY, USA: Harper & Row, 1985.

[51] T. K. Sarkar and O. Pereira, "Using the matrix pencil method to estimate the parameters of a sum of complex exponentials," *IEEE Antennas Propag. Mag.*, vol. 37, no. 1, pp. 48–55, Feb. 1995.

[52] M.-J. Park and S. Nam, "Rapid calculation of the Green's function in the shielded planar structures," *IEEE Trans. Microw. Guided Wave Lett.*, vol. 7, no. 10, pp. 326–328, Oct. 1997.

[53] K. Knopp, *Theory and Application of Infinite Series*. New York, NY, USA: Hafner, 1971.

[54] K. E. Jordan, G. R. Richter, and P. Sheng, "An efficient numerical evaluation of the Green's function for the Helmholtz operator on periodic structures," *J. Comput. Phys.*, vol. 63, pp. 222–235, 1986.

Brian J. Rautio (S'06) received the B.S.E.E. degree from the Rensselaer Polytechnic Institute, Troy, NY, USA, in 2009, and the M.S.E.E. degree from Syracuse University, Syracuse, NY, USA, in 2011, and is currently working toward the Ph.D. degree at Syracuse University, Syracuse, NY, USA.

He completed internships with Sonnet Software, North Syracuse, NY, USA, in 2005, 2007, and (part time) 2008, and with Advanced Micro Devices, Austin, TX, USA, in 2006. He is currently with Sonnet Software, North Syracuse , NY, USA.

Vladimir I. Okhmatovski (M'99–SM'09) was born in Moscow, Russia, in 1974. He received the M.S. degree (with distinction) in radiophysics and Ph.D. degree in antennas and microwave circuits from the Moscow Power Engineering Institute, Moscow, Russia, in 1996 and 1997, respectively.

In 1997, he joined the Radio Engineering Department, Moscow Power Engineering Institute, as an Assistant Professor. From 1998 to 1999, he was a Post-Doctoral Research Associate with the National Technical University of Athens. From 1999 to 2003, he was a Post-Doctoral Research Associate with the University of Illinois at Urbana-Champaign. From 2003 to 2004, he was with the Department of Custom Integrated Circuits, Cadence Design Systems, as a Senior Member of Technical Staff, and from 2004 to 2008, he was an independent Consultant. In 2004, he joined the Department of Electrical and Computer Engineering, University of Manitoba, Winnipeg, MB, Canada, where is currently an Associate Professor. He has coauthored over 80 refereed papers in journals and conference proceedings. His research interests are the fast algorithms of electromagnetics, high-performance computing, modeling of interconnects, and inverse problem.

Dr. Okhmatovski is a Registered Professional Engineer in the Province of Manitoba, Canada. He was the recipient of the 1995 scholarship of the Government of Russian Federation and the 1996 scholarship of the President of the Russian Federation. He was the recipient of the 1996 Best Young Scientist Report of the VI International Conference on Mathematical Methods in Electromagnetic Theory. He was also a corecipient of the Best Paper Award of the 3rd Electronic Packaging Technology Conference in 2001 and Outstanding ACES Journal Paper Award in 2007.

Andreas C. Cangellaris (F'00) received the Diploma degree in electrical engineering from the Aristotle University of Thessaloniki, Thessaloniki, Greece, in 1981, and the M.S. and Ph.D. degrees in electrical engineering from the University of California at Berkeley, Berkeley, CA, USA, in 1983 and 1985, respectively.

After a two-year tenure with the Electronics Department, General Motors Research Laboratories, he joined the Electrical and Computer Engineering (ECE) Department, University of Arizona, initially as an Assistant Professor (1987–1992) and then as an Associate Professor (1992–1997). In 1997, he joined the ECE Department, University of Illinois at Urbana-Champaign, Urbana, IL, USA, as a Full Professor in 1997, where he is currently the M. E. Van Valkenburg Professor and Dean of the College of Engineering. He has authored or coauthored over 250 papers in peer-reviewed journals and conference proceedings on the topics of finite methods for electromagnetic field modeling, multi-conductor transmission line modeling, and signal and power integrity of integrated electronic systems. His expertise and research interests are in applied and computational electromagnetics and its applications to the advancement of modeling methodologies and computer-aided design (CAD) tools in support of electrical performance analysis and noise-aware design of integrated electronic systems. His research group has conducted pioneering work in the advancement of modeling methodologies and computer tools for predictive electromagnetic response performance of the signal and the power distribution networks of integrated electronics at the board, package, and chip levels. Several of the prototype tools developed by his group have been transferred to the microelectronics industry and have contributed to the development of several EDA signal integrity tools.

Prof. Cangellaris was the cofounder of the IEEE Topical Meeting on Electrical Performance of Electronic Packaging in 1991. He is currently editor of the IEEE Press Series on Electromagnetic Wave Theory. He is an active member of the IEEE Microwave Theory and Techniques Society (IEEE MTT-S) and the IEEE Components Packaging and Manufacturing Technology Society, contributing to numerous professional activities, conferences, and symposia organized and sponsored by them. From 2010 to 2012, he was a Distinguished Lecturer for the IEEE MTT-S. He was the recipient of the 2000 University of Illinois, ECE Department Outstanding Faculty Teaching Award and the 2005 Alexander von Humboldt Research Award for outstanding contributions to electromagnetic theory.

James C. Rautio (S'77–M'78–SM'91–F'00) received the B.S.E.E. degree from Cornell University, Ithaca, NY, USA, in 1978, the M.S. degree in systems engineering from the University of Pennsylvania, Philadelphia, PA, USA, in 1982, and the Ph.D. degree in electrical engineering from Syracuse University, Syracuse, NY, USA, in 1986.

From 1978 to 1986, he was with General Electric, initially with the Valley Forge Space Division, then with the Syracuse Electronics Laboratory. During this time, he developed microwave design and measurement software and designed microwave circuits on alumina and on GaAs. From 1986 to 1988, he was a Visiting Professor with Syracuse University and Cornell University. In 1988, he joined Sonnet Software, Liverpool, NY, USA, full time, a company he had founded in 1983. In 1995, Sonnet Software was listed on the Inc. 500 list of the fastest growing privately held U.S. companies, the first microwave software company ever to be so listed. Today, Sonnet Software is the leading vendor of high-accuracy 3-D planar high-frequency electromagnetic analysis software.

Dr. Rautio was the recipient of the 2001 IEEE Microwave Theory and Techniques Society (IEEE MTT-S) Microwave Application Award. He was appointed an IEEE MTT-S Distinguished Microwave Lecturer for 2005–2007, during which time he was lectured on the life of James Clerk Maxwell.

Jay Kyoon Lee (S'80–M'85–SM'91) received the B.S. degree in electronics engineering from Seoul National University, Seoul, Korea, in 1976, and the S.M. and Ph.D. degrees in electrical engineering from the Massachusetts Institute of Technology, Cambridge, MA, USA, in 1981 and 1985, respectively.

In 1985, he joined the faculty of Department of Electrical Engineering and Computer Science at Syracuse University, Syracuse, NY, USA, where he is currently a Professor. From 2004 to 2009, he was the Program Director of Electrical Engineering with Syracuse University. During summers of 1987 and 1988, he was involved with the SAR imaging problem at the Naval Air Development Center, Warminster, PA, USA. In 1990, he was a Visiting Professor with the Rome Air Development Center, Rome, NY, USA. During the summer of 1993, he was also with the Naval Research Laboratory, Washington, DC, USA. In 2000, he was an Invited Visiting Professor with Seoul National University, Seoul, Korea. He has been on the International Editorial Board of the *Journal of Electromagnetic Waves and Applications* and *Progress in Electromagnetics Research (PIER)*. He coauthored *Electromagnetics* (Univ. Readers Inc., 2012). His teaching and research interests include electromagnetic fields and waves, microwave remote sensing, waves in anisotropic and gyrotropic media, antennas and propagation, and microwave engineering.

Dr. Lee is a member of the American Geophysical Union. He is a Fellow of the Electromagnetics Academy. He is a member of the Korean–American Scientists and Engineers Association (KSEA) in America. He has served as president of the Upstate New York Chapter of the KSEA (1990–1991), Faculty Advisor of the Korean Student Association, Syracuse University (since 1993), chair of the IEEE Syracuse Section (1995–1996), Student Activities Committee chair of IEEE Region 1 (1996–2000), and faculty advisor of the IEEE Student Branch, Syracuse University (since 1996). He was the recipient of the Eta Kappa Nu Outstanding Undergraduate Teacher Award from Syracuse University (1999), the IEEE Third Millennium Medal (2000), the College Educator of the Year Award from the Technology Alliance of Central New York (2002) and the IEEE Region 1 Award (2003).